Derivation of Symmetric Secant Stiffness Matrices for Nonlinear Finite Element Analysis

Paolo S. Valvo[1*]

[1] Department of Civil and Industrial Engineering, University of Pisa, Largo Lucio Lazzarino, I-56122 Pisa, Italy
* Corresponding author's e-mail: p.valvo@ing.unipi.it

ABSTRACT

Nonlinear finite element analysis requires the derivation of the secant elastic stiffness matrix of the discretised mechanical system. Most approaches of the literature lead to express the secant stiffness matrix as an asymmetric matrix, which then can be made symmetric by complicated numerical calculations or analytical formulae. The paper illustrates a straightforward method for the derivation of symmetric secant (and tangent) stiffness matrices for isoparametric finite elements made of hyper-elastic materials with both geometric and material nonlinearities. The method is based on the adoption of the nodal coordinates in the current configuration, instead of the nodal displacements, as the main unknowns. The method is illustrated in general for isoparametric elements with translational degrees of freedom. Specialised expressions and numerical examples are presented for truss bar elements and structures.

Keywords: finite element method, nonlinear analysis, stiffness matrix, isoparametric element, hyper-elastic material, absolute nodal coordinate formulation

INTRODUCTION

The increasing availability of light-weight and high-strength structural materials, in combination with advanced manufacturing techniques, has led to the conception of ever more enterprising and slender structures in modern aerospace, mechanical, and civil engineering applications [1–3]. As a matter of fact, the design of such advanced structures cannot be undertaken without resorting to numerical methods for structural analysis [4].

When a structural element undergoes displacements and deformations that overcome the limits acceptable for the validity of infinitesimal theory of elasticity, a nonlinear analysis must be conducted to accurately predict its mechanical behaviour [5–7]. In the finite element method (FEM), the nonlinear static equilibrium equations for a discretised, elastic mechanical system are generally stated in the following matrix form:

$$\mathbf{K}(\mathbf{u})\,\mathbf{u} - \mathbf{p} = \mathbf{0}, \qquad (1)$$

where: $\mathbf{K}$ – the secant elastic stiffness matrix of the system, depending on the nodal displacement vector $\mathbf{u}$, and
$\mathbf{p}$ – the nodal load vector [8].

Equations (1) can also be written as:

$$\mathbf{f}(\mathbf{u}) = \mathbf{p}, \qquad (2)$$

where:
$$\mathbf{f}(\mathbf{u}) = \mathbf{K}(\mathbf{u})\,\mathbf{u} \qquad (3)$$

is the nodal elastic force vector. Equations (2) highlight the fact that static equilibrium is a balance between the internal and external forces. Furthermore, from Equations (3), it follows that given two vectors $\mathbf{f}$ and $\mathbf{u}$, no unique definition of the secant stiffness matrix exists. Indeed, $\mathbf{K}(\mathbf{u})$ can be expressed as either a symmetric or an asymmetric matrix. It is clear that having a symmetric matrix is desirable to reduce the use of computer memory and to improve the computational effectiveness of solution algorithms.

In linear analysis, i.e., for small strains and displacements, the stiffness matrix $\mathbf{K}$ is evaluated in the reference configuration of the system

independently of the nodal displacements. In this case, the stiffness matrix is always a symmetric matrix. Instead, in geometrically nonlinear analysis, i.e., when strains and displacements may attain large values, $\mathbf{K}$ must be evaluated in the current configuration and depends on the nodal displacements. In the literature, several strategies have been proposed for the evaluation of the secant stiffness matrix [9, 10]. Most approaches lead to express $\mathbf{K}$ as an asymmetric matrix, which then can be made symmetric by suitable manipulations [11]. Also, it should be noted that most approaches of the literature are based on complicated numerical calculations or analytical formulae.

The paper illustrates a straightforward method for the derivation of symmetric secant stiffness matrices for systems made of hyper-elastic materials characterised by both geometric and material nonlinearities. The method is based on the adoption of the nodal coordinate vector in the current configuration $\mathbf{x}$, instead of the nodal displacement vector $\mathbf{u}$, as the main unknown. As a result, the nodal internal force vector is expressed as:

$$\mathbf{f}(\mathbf{x}) = \mathbf{S}(\mathbf{x})\,\mathbf{x}, \tag{4}$$

where: $\mathbf{S}$ – a symmetric secant stiffness matrix depending on the nodal coordinate vector.

The proposed approach turns out to be similar to the absolute nodal coordinate formulation (ANCF) used for flexible multibody dynamics [12], here adapted to the context of computational solid and structural mechanics. In what follows, first the method is presented for general isoparametric finite elements with translational degrees of freedom. Then, specialised expressions are deduced for the truss bar element. Lastly, the effectiveness of the method is illustrated by the analysis of some well-known planar and spatial truss structures.

ANALYTICAL DERIVATION OF STIFFNESS MATRICES

Finite element formulation

Let us consider the nonlinear static equilibrium problem for a continuous body made of a hyper-elastic material and occupying a region Ω of the Euclidean space of dimension d. In the finite element formulation (Figure 1), the region Ω is approximated by the union of m regions, $\Omega_1, \Omega_2, \ldots, \Omega_m$, corresponding to the finite

elements. Elements are connected to each other and to the support only at a discrete number n of points called nodes. Also, the distributed surface and body forces, as well as the kinematic restraints, of the continuous model are substituted by their equivalent, concentrated nodal loads and restraints [8].

Let us fix a Cartesian reference system $Ox_1 \ldots x_d$. Thus, physical vectors can be represented in terms of their real-valued components as column vectors of R^d (here and in the following, R denotes the set of real numbers). Besides, let us choose a reference configuration $\bar{\Omega}$ as one of the many configurations that the body can occupy. Let $\bar{P} \in \bar{\Omega}$ be the point corresponding to a given material particle in the reference configuration and $P \in \Omega$ the point corresponding to the same particle in the current configuration. We denote with $\bar{\mathbf{x}}_P = \bar{P} - O$ and $\mathbf{x}_P = P - O$ the position vectors of the two points. Besides,

$$\mathbf{u}_P = P - \bar{P} = \mathbf{x}_P - \bar{\mathbf{x}}_P \tag{5}$$

denotes the displacement vector of the considered particle.

The displacement vector field defined over the reference configuration represents the main unknown of the continuous problem. In the standard finite element formulation, the displacement field within each element is approximated by a suitable interpolation of the displacement vectors of the nodes connected to the element. In particular, for an isoparametric element with only translational degrees of freedom, the displacement vector field can be represented as:

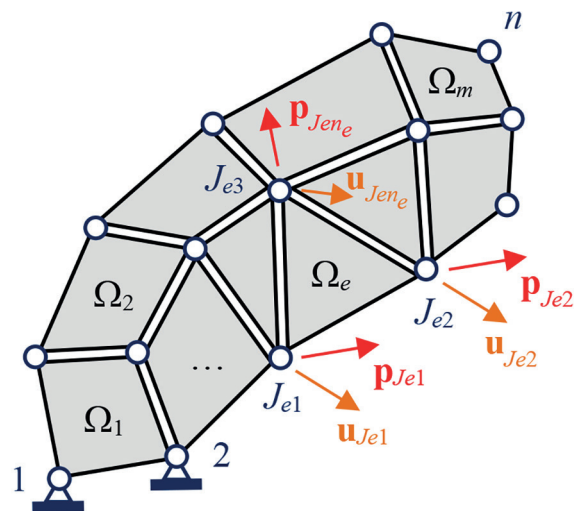$$\mathbf{u}_P \cong \mathbf{N}_e(\bar{\mathbf{x}}_P)\,\mathbf{u}_e, \tag{6}$$

Figure 1. Finite element model of a continuous elastic body

where: e – the element label,

$\mathbf{N}_e(\overline{\mathbf{x}}_P) \in \mathbb{R}^{d \times n_e d}$ – the shape function matrix of the element and

$\mathbf{u}_e = [\mathbf{u}_{J_{e1}}; \mathbf{u}_{J_{e2}}; \ldots; \mathbf{u}_{J_{e n_e}}] \in \mathbb{R}^{n_e d}$ – the nodal displacement vector of the element. Here, $J_{e1}, J_{e2}, \ldots, J_{e n_e}$ – the labels of the nodes of the element and n_e is their total number.

The nodal displacement vector of the element can also be expressed as follows:

$$\mathbf{u}_e = \mathbf{A}_e \mathbf{u}, \qquad (7)$$

where: $\mathbf{A}_e \in \mathbb{R}^{n_e d \times nd}$ and $\mathbf{u} = [\mathbf{u}_1; \mathbf{u}_2; \ldots; \mathbf{u}_n] \in \mathbb{R}^{nd}$ respectively are the assembly matrix of the element and the displacement vector of the system. The assembly matrix $\mathbf{A}_e$ has all null entries, except for the macro-rows and macro-columns corresponding to the element nodes, where identity matrices $\mathbf{I} \in \mathbb{R}^{d \times d}$ are placed. The displacement vector $\mathbf{u}$ collects the displacement components of all of the nodes of the model and constitutes the main unknown of the discretised problem. It should be noted that while the assembly matrix is useful for the analytical formulation, in numerical implementation it is more computationally effective to code the assembly process via direct extraction of the sub-vectors and sub-matrices corresponding to the involved nodes [13].

For what follows, it is also useful to introduce the nodal position vectors of the element $\overline{\mathbf{x}}_e = [\overline{\mathbf{x}}_{J_{e1}}; \overline{\mathbf{x}}_{J_{e2}}; \ldots; \overline{\mathbf{x}}_{J_{e n_e}}] = \mathbf{A}_e \overline{\mathbf{x}} \in \mathbb{R}^{n_e d}$ and $\mathbf{x}_e = [\mathbf{x}_{J_{e1}}; \mathbf{x}_{J_{e2}}; \ldots; \mathbf{x}_{J_{e n_e}}] = \mathbf{A}_e \mathbf{x} \in \mathbb{R}^{n_e d}$ in the reference and current configurations, respectively. In line with the notation used for the displacements, $\overline{\mathbf{x}} = [\overline{\mathbf{x}}_1; \overline{\mathbf{x}}_2; \ldots; \overline{\mathbf{x}}_n] \in \mathbb{R}^{nd}$ and $\mathbf{x} = [\mathbf{x}_1; \mathbf{x}_2; \ldots; \mathbf{x}_n] \in \mathbb{R}^{nd}$ respectively are the nodal position vectors of the system in the reference and current configurations.

Green-Lagrange strain measure

In the presence of large strains and displacements, the deformation can be conveniently measured by using the Green-Lagrange strain tensor [14]. For an element with dimension d_e, the Cartesian components of the strain tensor turn out to be:

$$E_{\alpha\beta} = \frac{1}{2}\left[\left(\frac{\partial \mathbf{x}_P}{\partial s_\alpha}\right)^{\mathrm{T}} \frac{\partial \mathbf{x}_P}{\partial s_\beta} - \left(\frac{\partial \overline{\mathbf{x}}_P}{\partial s_\alpha}\right)^{\mathrm{T}} \frac{\partial \overline{\mathbf{x}}_P}{\partial s_\beta}\right], \quad (8)$$

where: s_α and s_β are local coordinates for the element with the indices α and β ranging

from 1 to d_e. By introducing Equations (5) and (6) into (8), after some manipulations, the expression for the strain components can be put in the following form:

$$E_{\alpha\beta} = \frac{1}{2}(\mathbf{x}_e + \overline{\mathbf{x}}_e)^{\mathrm{T}} \mathbf{\Gamma}_{\alpha\beta}(\mathbf{x}_e - \overline{\mathbf{x}}_e), \qquad (9)$$

where: the symmetric matrices

$$\mathbf{\Gamma}_{\alpha\beta} = \frac{1}{2}\left[\left(\frac{\partial \mathbf{N}_e}{\partial s_\alpha}\right)^{\mathrm{T}} \frac{\partial \mathbf{N}_e}{\partial s_\beta} + \left(\frac{\partial \mathbf{N}_e}{\partial s_\beta}\right)^{\mathrm{T}} \frac{\partial \mathbf{N}_e}{\partial s_\alpha}\right] \in \mathbb{R}^{n_e d \times n_e d} \qquad (10)$$

have been introduced. For what follows, it will be useful to calculate the derivative of the strains:

$$\frac{\partial E_{\alpha\beta}}{\partial \mathbf{x}_e} = \mathbf{\Gamma}_{\alpha\beta} \mathbf{x}_e. \qquad (11)$$

Nonlinear static equilibrium equations

The nonlinear static equilibrium equations can be deduced by imposing the stationarity of the total potential energy of the system [15]:

$$\mathcal{V} = \mathcal{U} - \mathcal{W}, \qquad (12)$$

where: $\mathcal{U}$ is the strain energy stored in the whole system and

$\mathcal{W}$ is the virtual work done by the loads. Such contributions can be calculated as explained in the following.

The mechanical response of hyper-elastic materials is characterised by the definition of a potential function $\overline{\varphi} = \overline{\varphi}(E_{\alpha\beta})$, from which the stress-strain relationships are derived. In particular, the work-conjugate stress measure for the Green-Lagrange strain tensor is the second Piola-Kirchhoff stress tensor [14], whose components turn out to be

$$S_{\alpha\beta} = \frac{\partial \overline{\varphi}}{\partial E_{\alpha\beta}}. \qquad (13)$$

Besides, $\overline{\varphi}$ can be interpreted as the strain-energy density, i.e. the strain energy stored in a unit volume in the reference configuration. Thus, the strain energy stored in an element e is:

$$\mathcal{U}_e = \int_{\overline{\Omega}_e} \overline{\varphi} \, \mathrm{d}\overline{V} \qquad (14)$$

and the strain energy of the whole system is given by:

$$\mathcal{U} = \sum_{e=1}^{m} \mathcal{U}_e. \qquad (15)$$

Besides, it is assumed that the load vector can be expressed as:

$$\mathbf{p} = \lambda \overline{\mathbf{p}} \qquad (16)$$

where λ is a scalar load multiplier and $\bar{\mathbf{p}}$ is a reference nodal load vector. As a consequence, the virtual work of the loads turns to be:

$$\mathscr{W} = \mathbf{p}^{\mathrm{T}}\mathbf{u} = \lambda\bar{\mathbf{p}}^{\mathrm{T}}(\mathbf{x} - \bar{\mathbf{x}}). \tag{17}$$

By differentiating Equation 12, the nonlinear equilibrium equations are obtained:

$$\mathbf{g}(\mathbf{x}) = \frac{\partial\mathscr{V}}{\partial\mathbf{x}} = \frac{\partial\mathscr{U}}{\partial\mathbf{x}} - \frac{\partial\mathscr{W}}{\partial\mathbf{x}} = \mathbf{f}(\mathbf{x}) - \mathbf{p} = \mathbf{0}, \tag{18}$$

where, by recalling also Equations (14)–(17), the nodal elastic force vector is:

$$\mathbf{f}(\mathbf{x}) = \frac{\partial\mathscr{U}}{\partial\mathbf{x}} = \frac{\partial}{\partial\mathbf{x}}\sum_{e=1}^{m}\mathscr{U}_e = \frac{\partial}{\partial\mathbf{x}}\sum_{e=1}^{m}\int_{\bar{\Omega}_e}\bar{\varphi}\,\mathrm{d}\bar{V} \tag{19}$$

and the nodal load vector is:

$$\mathbf{p} = \frac{\partial\mathscr{W}}{\partial\mathbf{x}} = \lambda\bar{\mathbf{p}}. \tag{20}$$

Symmetric secant elastic stiffness matrices

By applying the chain rule for differentiation and recalling Equation (7), from Equation (19), the nodal elastic force vector is obtained:

$$\mathbf{f}(\mathbf{x}) = \sum_{e=1}^{m}\int_{\bar{\Omega}_e}\sum_{\alpha=1}^{d_e}\sum_{\beta=1}^{d_e}\frac{\partial E_{\alpha\beta}}{\partial\mathbf{x}}\frac{\partial\bar{\varphi}}{\partial E_{\alpha\beta}}\,\mathrm{d}\bar{V} = \sum_{e=1}^{m}\mathbf{A}_e^{\mathrm{T}}\mathbf{f}_e(\mathbf{x}_e), \tag{21}$$

where:

$$\mathbf{f}_e(\mathbf{x}_e) = \int_{\bar{\Omega}_e}\sum_{\alpha=1}^{d_e}\sum_{\beta=1}^{d_e}\frac{\partial E_{\alpha\beta}}{\partial\mathbf{x}_e}\frac{\partial\bar{\varphi}}{\partial E_{\alpha\beta}}\,\mathrm{d}\bar{V} \tag{22}$$

is the nodal elastic force vector of element e.

By substituting Equation (13) into (22) and recalling Equation (11), the nodal elastic force vector for the element can be expressed as:

$$\mathbf{f}_e(\mathbf{x}_e) = \mathbf{S}_e(\mathbf{x}_e)\,\mathbf{x}_e, \tag{23}$$

where:

$$\mathbf{S}_e(\mathbf{x}_e) = \int_{\bar{\Omega}_e}\sum_{\alpha=1}^{d_e}\sum_{\beta=1}^{d_e}S_{\alpha\beta}\boldsymbol{\Gamma}_{\alpha\beta}\,\mathrm{d}\bar{V} \in \mathsf{R}^{n_ed \times n_ed} \tag{24}$$

is the symmetric secant elastic stiffness matrix of the element, expressed as a function of the nodal position vector. By substituting Equations (23) into (21) and recalling Equation (11), the nodal elastic force vector for the whole system is obtained as:

$$\mathbf{f}(\mathbf{x}) = \mathbf{S}(\mathbf{x})\,\mathbf{x}, \tag{25}$$

where:

$$\mathbf{S}(\mathbf{x}) = \sum_{e=1}^{m}\mathbf{A}_e^{\mathrm{T}}\,\mathbf{S}_e(\mathbf{x}_e)\,\mathbf{A}_e \in \mathsf{R}^{nd \times nd} \tag{26}$$

is the symmetric secant elastic stiffness matrix of the system, expressed as a function of the nodal position vector. By substituting Equations (20) and (25) into (18), the nonlinear equilibrium equations are finally obtained in the following form:

$$\mathbf{g}(\mathbf{x}) = \mathbf{S}(\mathbf{x})\,\mathbf{x} - \lambda\bar{\mathbf{p}} = \mathbf{0}, \tag{27}$$

where the main unknown is the nodal position vector $\mathbf{x}$, instead of the displacement vector $\mathbf{u}$.

The implementation of incremental-iterative solution methods also requires the introduction of the tangent stiffness matrix of the system, which can be calculated as follows:

$$\mathbf{T}(\mathbf{x}) = \frac{\partial\mathbf{f}}{\partial\mathbf{x}} = \frac{\partial[\mathbf{S}(\mathbf{x})\,\mathbf{x}]}{\partial\mathbf{x}} = \sum_{e=1}^{m}\mathbf{A}_e^{\mathrm{T}}\,\mathbf{T}_e(\mathbf{x}_e)\,\mathbf{A}_e \in \mathsf{R}^{nd \times nd}, \tag{28}$$

where

$$\mathbf{T}_e(\mathbf{x}_e) = \mathbf{S}_e(\mathbf{x}_e) +$$
$$+ \int_{\bar{\Omega}_e}\sum_{\alpha=1}^{d_e}\sum_{\beta=1}^{d_e}\sum_{\gamma=1}^{d_e}\sum_{\delta=1}^{d_e}\frac{\partial^2\bar{\varphi}}{\partial E_{\alpha\beta}\partial E_{\gamma\delta}}\boldsymbol{\Gamma}_{\alpha\beta}\,\mathbf{x}_e\mathbf{x}_e^{\mathrm{T}}\,\boldsymbol{\Gamma}_{\gamma\delta}\,\mathrm{d}\bar{V} \in \mathsf{R}^{n_ed \times n_ed} \tag{29}$$

is the tangent stiffness matrix of element e.

In closure, it is noted that the volume integrals appearing in Equations (24) and (29) can be carried out numerically, if necessary [8].

Explicit expressions for the truss bar element

The general expressions of the secant stiffness matrices are now specialised to an isoparametric truss bar element. The formulation will be valid for both planar ($d = 2$) and spatial ($d = 3$) structures.

Let us consider a truss bar element labelled e with $n_e = 2$ nodes J_{e1} and J_{e2}. Let $\bar{A}_e$ and $\bar{L}_e$ respectively denote the truss bar cross-section area and length in the element reference configuration $\bar{\Omega}_e$. The element has dimension $d_e = 1$ and a local coordinate $s_1 \in [0, \bar{L}_e]$ is fixed along the bar centreline (Figure 2).

The displacement field is assumed to be described by linear shape functions:

$$N_{e1}(s_1) = 1 - \frac{s_1}{\bar{L}_e} \text{ and } N_{e2}(s_1) = \frac{s_1}{\bar{L}_e}. \tag{30}$$

and the shape function matrix is defined as follows:

$$\mathbf{N}_e(s_1) = \begin{bmatrix} N_{e1}(s_1)\mathbf{I} & N_{e2}(s_1)\mathbf{I} \end{bmatrix}, \tag{31}$$

where: $\mathbf{I} \in \mathsf{R}^{d \times d}$ is the identity matrix. The derivative of the shape function matrix turns out to be:

$$\frac{\partial\mathbf{N}_e}{\partial s_1} = \frac{1}{\bar{L}_e}\begin{bmatrix} -\mathbf{I} & \mathbf{I} \end{bmatrix}. \tag{32}$$

Thus, the matrix defined in Equation (10) can be easily calculated (since the element is 1-dimensional, indices $\alpha = \beta = 1$):

$$\boldsymbol{\Gamma}_{11} = \frac{1}{\bar{L}_e^2}\boldsymbol{\Delta}, \tag{33}$$
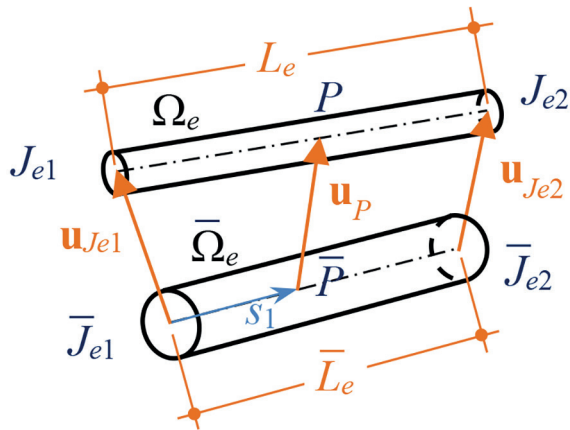
Figure 2. Truss bar element

where the following constant matrix is introduced:

$$\mathbf{\Delta} = \begin{bmatrix} \mathbf{I} & -\mathbf{I} \\ -\mathbf{I} & \mathbf{I} \end{bmatrix} \in \mathsf{R}^{2d \times 2d}. \quad (34)$$

The axial strain in the truss bar can be calculated from Equation (9):

$$E_{11} = \frac{1}{2} \frac{1}{\overline{L}_e^2} (\mathbf{x}_e + \overline{\mathbf{x}}_e)^{\mathrm{T}} \mathbf{\Delta} (\mathbf{x}_e - \overline{\mathbf{x}}_e). \quad (35)$$

In passing, it is noted that the axial strain, as well as the corresponding stress S_{11}, turns out to be constant because of the linearity of the assumed shape functions. This result simplifies the integration over the volume of the element and avoids the use of numerical integration procedures. In particular, by substituting Equation (33) into (24) and performing the integration over the reference volume of the element $\overline{V}_e = \overline{A}_e \overline{L}_e$, the element secant stiffness matrix is obtained:

$$\mathbf{S}_e(\mathbf{x}_e) = \int_{\overline{\Omega}_e} \sum_{\alpha=1}^{1} \sum_{\beta=1}^{1} S_{\alpha\beta} \mathbf{\Gamma}_{\alpha\beta} \, \mathrm{d}\overline{V} = S_{11} \frac{\overline{A}_e}{\overline{L}_e} \mathbf{\Delta}. \quad (36)$$
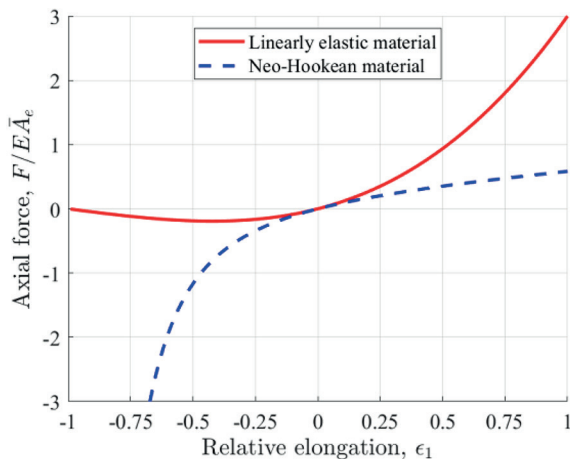

Figure 3. Axial-force vs. relative elongation

Furthermore, Equation (29) for the element tangent stiffness matrix specialises to:

$$\mathbf{T}_e(\mathbf{x}_e) = \mathbf{S}_e(\mathbf{x}_e) + \frac{\partial S_{11}}{\partial E_{11}} \frac{\overline{A}_e}{\overline{L}_e^3} \mathbf{\Delta} \, \mathbf{x}_e \mathbf{x}_e^{\mathrm{T}} \mathbf{\Delta}. \quad (37)$$

It is worth noting that Equations (36) and (37) are valid not only for linearly elastic materials, but also for any type of nonlinear hyper-elastic material [14].

NUMERICAL EXAMPLES

Material laws

For the sake of illustration, two ideal materials are considered for the truss bars [14]:
1) a linearly elastic material, for which the strain-energy density is:

$$\overline{\varphi}(E_{11}) = \frac{1}{2} E E_{11}^2, \quad (38)$$

where: E is the Young's modulus;

2) an incompressible neo-Hookean material, for which the strain-energy density is:

$$\overline{\varphi}(E_{11}) = \frac{1}{2} \mu \left(\lambda_1^2 + 2\lambda_1^{-1} - 3 \right), \quad (39)$$

where: $\mu = E/3$ is the shear modulus and $\lambda_1 = \sqrt{2E_{11} + 1}$ is the stretch in the bar axial direction.

In the two cases, Equation (13) for the second Piola-Kirchhoff stress specialises as follows:

$$S_{11} = E E_{11} \text{ with } \frac{\partial S_{11}}{\partial E_{11}} = E \quad (40)$$

and

$$S_{11} = \frac{1}{3} E \left(1 - \lambda_1^{-3} \right) \text{ with } \frac{\partial S_{11}}{\partial E_{11}} = E \lambda_1^{-5}, \quad (41)$$

respectively.

Figure 3 shows a plot of the axial force $F = \lambda_1 S_{11} \overline{A}_e$ vs. the relative elongation $\varepsilon_1 = (L_e - \overline{L}_e)/\overline{L}_e = \lambda_1 - 1$ of a truss bar, according to the two considered material laws.

Von Mises' truss

As a first example, the planar von Mises' truss shown in Figure 4 is analysed. Despite its simplicity, this structure can exhibit a wide range of instability phenomena [16]. Therefore, thanks to the availability of analytical solutions, it has been widely used for the validation of numerical

solution algorithms [19]. Recently, Fonseca and Gonçalves [20] have presented an analytical solution for the von Mises' truss with bars made of nonlinear hyper-elastic materials.

The following numerical values are used in this example: $b = 250$ mm, $E = 200$ GPa, $\bar{A}_e = 100$ mm^2, $(\bar{\mathbf{p}}_1)_1 = 200$ kN; two values are considered for the height: $h = 100$ mm and $h = 500$ mm, respectively corresponding to a shallow truss and a deep truss. The equilibrium paths, i.e. the curves representing the equilibrium configurations in the load-displacement space, have been obtained by using the arc-length method [17, 18] with the admissible direction cone constraint proposed by Ligarò and Valvo [19].

Figure 5 shows the paths obtained for the shallow and deep trusses with both linearly elastic and neo-Hookean materials. For the shallow truss, the overall structural response changes only marginally because of the different material laws adopted. Instead, for the deep truss, remarkable differences in the structural response are observed

due to the different material laws. For the deep truss, it is known that also bifurcation points and a secondary branch are present on the equilibrium path [16, 19, 20]. However, their detection and tracing are not described here, as not being related to the main scope of the present work.

Star-shaped dome

As a second example, the star-shaped dome shown in Figure 6 is considered. This three-dimensional structure has been investigated first by Abatan and Holzer [21] and later used by many Authors as a benchmark test.

The following numerical values are assumed: $r_1 = 250$ mm, $r_2 = 500$ mm, $h_1 = 20$ mm, $h_2 = 82.16$ mm, $E = 200$ GPa, $\bar{A}_e = 100$ mm^2, $(\bar{\mathbf{p}}_1)_3 = 20$ kN. As for the previous example, the equilibrium path has been obtained by using the method by Ligarò and Valvo [19].

Figure 7 shows the equilibrium path of the dome traced by assuming linearly elastic and
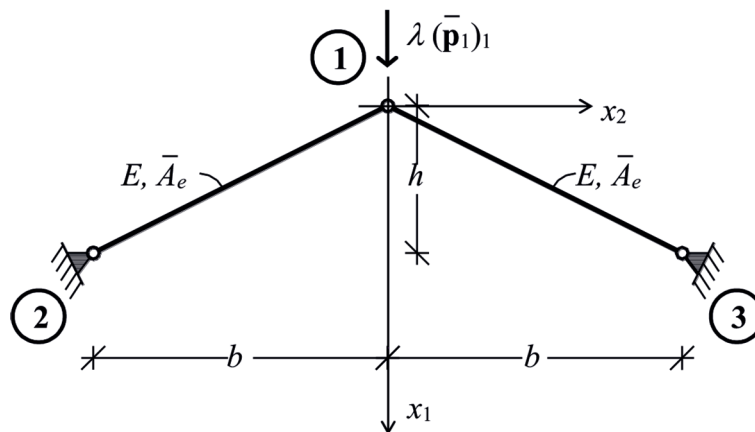

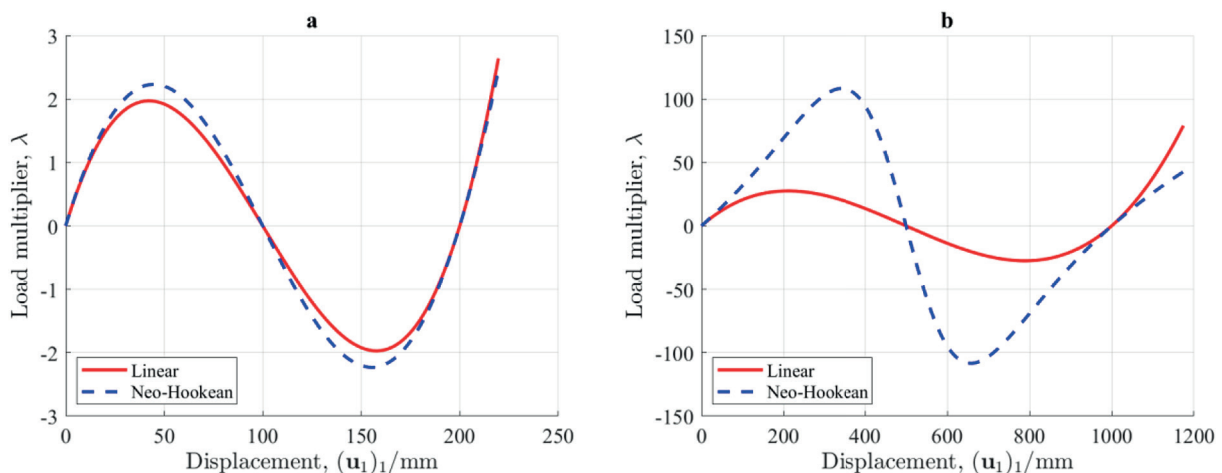**Figure 4.** Von Mises' truss: reference configuration

Figure 5. Equilibrium paths of a) shallow and b) deep von Mises' trusses

neo-Hookean material laws. For this structure, the overall response changes only marginally because of the different material laws adopted. Anyway, the effectiveness of the proposed formulation is demonstrated. Also, it should be noted that the complete equilibrium path of this structure features some bifurcation points and secondary branches [19]. However, their detection and tracing are omitted here, as not being related to

the main scope of the present work. The equilibrium path of the dome is a curve in a 22-dimensional space (1 load multiplier + 21 displacement components of the free nodes). Figures 7a and 7b show projections of such curve onto two selected planes. The apparent self-intersections of the path in Figure 7a do not correspond to bifurcation points. In fact, the same curve projected onto a different plane appears as a simple curve (Figure 7b). Lastly, it is noted that one value of vertical displacement of the central node 1 may occur at several values of the load multiplier (Figure 7a), because these correspond in fact to different deformed configurations of the structure.

CONCLUSIONS

General analytic expressions have been deduced for the secant and tangent stiffness matrices of isoparametric finite elements made of hyper-elastic materials. Such symmetric matrices are useful for the finite element analysis of elasticity problems characterised by both geometric and material nonlinearities. Specialised expressions of the stiffness matrices have been presented for the truss bar element. Then, the effectiveness of the proposed formulation has been demonstrated for the nonlinear static analysis of some well-known examples of planar and spatial truss structures.

The same formulation for the stiffness matrices can be usefully exploited also for nonlinear dynamic analysis. As a first application, the dynamic deployment of a cable net has been recently investigated [22].
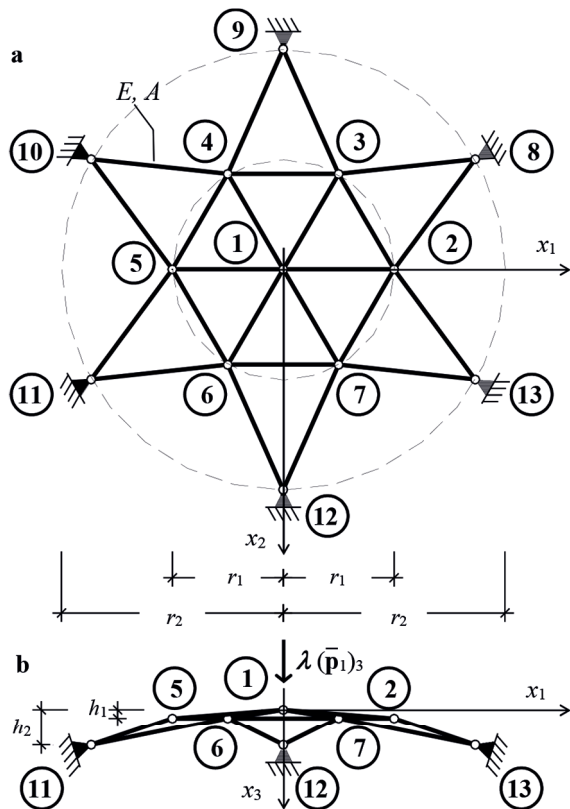

Figure 6. Star-shaped dome: a) plan view and b) side view in the reference configuration
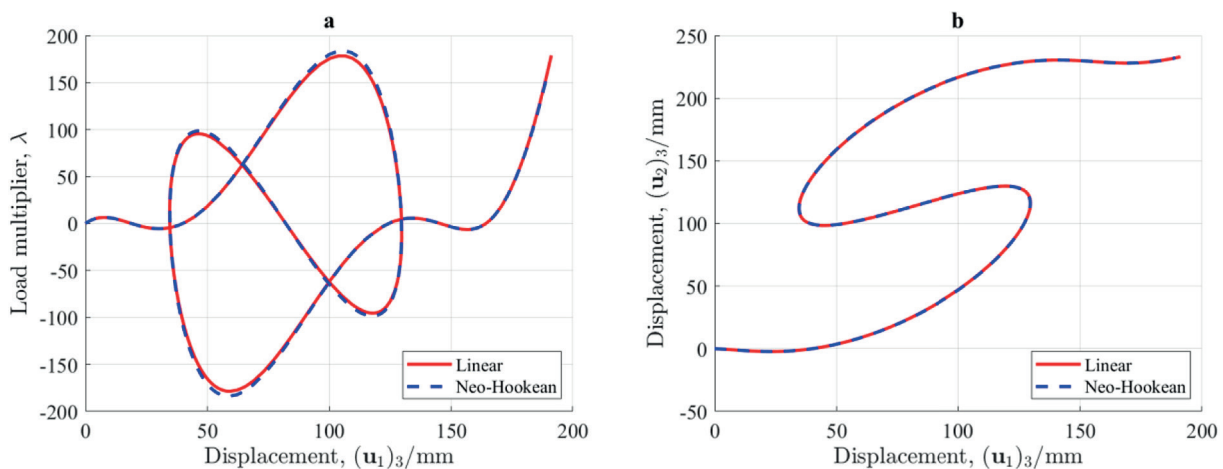

Figure 7. Equilibrium path of the star-shaped dome: a) load multiplier vs. node 1 vertical displacement and b) node 2 vertical displacement vs. node 1 vertical displacement

Specialisation to more general isoparametric elements for the analysis of two- and three-dimensional elasticity problems, as well as the extension to elements with rotational degrees of freedom, will be the subject of future developments.

REFERENCES

1. Li Y., Xiao Y., Yu L., Ji K., Li D. A review on the tooling technologies for composites manufacturing of aerospace structures: materials, structures and processes. Composites Part A: Applied Science and Manufacturing 2022; 154: 106762.

2. Zhang W., Xu J., Yu T.X. Dynamic behaviors of bio-inspired structures: Design, mechanisms, and models. Engineering Structures 2022; 265: 114490.

3. Xu J., Zhang Y., Yu Q., Zhang, L. Analysis and design of fabric membrane structures: A systematic review on material and structural performance. Thin-Walled Structures 2022; 170: 108619.

4. Eisley J.G., Waas A.M. Analysis of Structures: An Introduction Including Numerical Methods. Wiley, 2011.

5. Kopecki T., Lis T., Mazurek P., Bakunowicz J. Buckling Deformation of Thin Layer Coverings of Small Curvatures Used in Aircraft Construction. Advances in Science and Technology Research Journal 2018; 12(1): 293–302.

6. Kopecki T., Lis T., Mazurek P. Post-critical Deformation of Thin-Walled Load-Bearing Aircraft Structure Representing Fragment of the One-Way Torsion Box. Advances in Science and Technology Research Journal 2018; 12(3): 203–209.

7. Kopecki T. Selected Methods of Obtaining Adequate Forms of Deformation of Supercritical Thin-Walled Flat Plates. Advances in Science and Technology Research Journal 2021; 15(2): 184–190.

8. Wriggers P. Nonlinear Finite Element Methods. Springer, 2008.

9. Moran A., Oñate E., Miquel J. A general procedure for deriving symmetric expressions for the secant and tangent stiffness matrices in finite element analysis. International Journal for Numerical Methods in Engineering 1998; 42(2): 219–236.

10. Pedersen P. Analytical stiffness matrices with Green–Lagrange strain measure. International Journal for Numerical Methods in Engineering 2005; 62(3): 334–352.

11. Oñate E. On the derivation and possibilities of the secant stiffness matrix for non linear finite element analysis. Computational Mechanics 1995; 15(6): 572–593.

12. Shabana A.A. Computer implementation of the absolute nodal coordinate formulation for flexible multibody dynamics. Nonlinear Dynamics 1998; 16: 293–306.

13. Kuna M. Finite Elements in Fracture Mechanics. Springer, 2013.

14. Ogden R.W. Non-linear Elastic Deformations. Dover, 1985.

15. Bažant Z.P., Cedolin L. Stability of Structures. Oxford University Press, 1991.

16. Pecknold D.A., Ghaboussi J., Healey T.J. Snap-through and bifurcation in a simple structure. ASCE Journal of Engineering Mechanics 1985; 111(7): 909–922.

17. Riks E., An incremental approach to the solution of snapping and buckling problems. International Journal of Solids Structures 1979; 15(7): 529–551.

18. Crisfield M.A. A fast incremental/iterative solution procedure that handles snap-through. Computers & Structures 1981; 13(1–3): 55–62.

19. Ligarò S., Valvo P. A self-adaptive strategy for uniformly accurate tracing of the equilibrium paths of elastic reticulated structures. International Journal for Numerical Methods in Engineering 1999; 46(6): 783–804.

20. Fonseca F.M, Gonçalves P.B. Nonlinear behavior and instabilities of a hyperelastic Von Mises truss. International Journal of Non-Linear Mechanics 2022; 142: 103964.

21. Abatan A.O., Holzer S.M. Degree of stability of geodesic domes with independent loading parameters. Computers and Structures 1978; 9(1): 43–51.

22. Fisicaro P., Pasini A., Valvo P.S. Simulation of Deployable Cable Nets for Active Debris Removal in Space. Journal of Physics: Conference Series 2022.